JOURNAL OF
biomaterials
applications

Biomaterials Processing

Journal of Biomaterials Applications
2020, Vol. 34(9) 1201–1215

DOI: 10.1177/0885328220901987
journals.sagepub.com/home/jba
SAGE

Fish scale/poly(3-hydroxybutyrate-*co*-3-hydroxyvalerate) nanofibrous composite scaffolds for bone regeneration

Aylin Kara[1], Oylum C Gunes[2], Aylin Z Albayrak[2], Gokcen Bilici[3], Guven Erbil[3] and Hasan Havitcioglu[4]

Abstract

The aim of this study was to produce three-dimensional, nanofibrous fish scale/poly(3-hydroxybutyrate-*co*-3-hydroxyvalerate) composite scaffolds as bone filling materials. This is the first report wherein fish scales were used within a nanofibrous matrix for bone regeneration. Composite scaffolds with a cotton wool-like structure (fiber diameter: 560 ± 64 nm; porosity: 82%) were obtained by incorporating chopped fish scales into wet-electrospun poly(3-hydroxybutyrate-*co*-3-hydroxyvalerate) nanofibers and freeze-drying. The addition of the fish scales improved the mechanical properties, biomineralization tendency, cell viability, alkaline phosphatase activity, and type I collagen production. Consequently, produced composite scaffolds would be regarded to have the therapeutic capacity in bone tissue damages.

Keywords

Fish scale, scaffold, PHBV, wet-electrospinning, bone regeneration, bone filling material

Introduction

In bone tissue engineering, scaffolds are required to be porous, biocompatible, bioactive, and biodegradable. Mechanical strength of the scaffold should be high enough until the newly formed tissues are structurally stable. They should also have three-dimensional fibrous structure that mimic the bone extracellular matrix (ECM).[1–3]

Bone ECM is a nanocomposite that consists of nano-hydroxyapatite (HAp) and type I collagen fibrils.[4,5] The elasmoid scales of teleost fish are highly ordered three-dimensional structure and composed of ECM, mainly type I collagen fibers and HAp similar to bone tissue.[6] The scales consist of two layers: external (osseous) layer with randomly arranged collagen fibers and fibrillary internal (basal plate) layer where collagen fibers are organized into lamellae to produce an orthogonal and/or a double-twisted plywood-like pattern.[6,7] The distinct organization of fibers is the key factor for improved mechanical properties.[6,8] Mineralization of the scales occurs with the accumulation of the HAp between collagen fibers. Needle-like HAp crystals were distributed through the aligned collagen fibers in the internal layer of the fish scale.[9]

The studies about fish scales generally consist of the extraction of collagen[10–13] and HAp[14–16] for producing scaffolds for bone tissue engineering[14,16,17] or artificial cornea.[11] Besides, there are studies on the evaluating biocompatibility of fish scales. Fang et al.[18] studied the structure and the cytocompatibility of fish scales from *Carassius auratus*. Cell culture results showed a high cytocompatibility and the ability to guide cell proliferation and migration on the fish scales. They also claimed that the plywood structure of the scales could be an inspiration for a structure-enhanced composite material.[18] Moreover, Yamamoto et al.[19] reported that the fish scale, skin, and bone derived collagen is a biologically safe material. However, there is no study which involves scaffold comprising intact fish scale.

[1]Biotechnology and Bioengineering Program, The Graduate School of Engineering & Sciences, Izmir Institute of Technology, Izmir, Turkey
[2]Department of Metallurgical and Materials Engineering, Faculty of Engineering, Dokuz Eylul University, Izmir, Turkey
[3]Department of Histology and Embryology, Faculty of Medicine, Dokuz Eylul University, Izmir, Turkey
[4]Department of Orthopedics and Traumatology, Faculty of Medicine, Dokuz Eylul University, Izmir, Turkey

Corresponding author:
Aylin Z Albayrak, Faculty of Engineering, Dokuz Eylul University, Tınaztepe Campus, Izmir 35390, Turkey.
Email: aylin.albayrak@deu.edu.tr

Fish scales are actually biodegradable waste material, but the structural similarity to the bone ECM is valuable for tissue engineering applications.

Nanofibrous scaffolds have been widely used in bone tissue engineering applications in order to resemble the main structure of bone ECM.[20] There are many methods to produce nanofibrous scaffolds, but among them, electrospinning is considered as the simplest and the most widely studied one.[21] However, two-dimensional nanofibrous mats produced by electrospinning are not enough for cell–cell interaction, cell migration, and cell morphogenesis. The wet-electrospinning method has been developed to produce three-dimensional nanofibrous cotton wool-like scaffolds to overcome the limitation of electrospinning method. In this method, polymer solution is first electrospun into the coagulation bath including a low surface tension solvent, and then homogeneously suspended fibers are collected and freeze-dried to maintain the three-dimensional structure.[22,23]

Co-polymers (PLGA, PHBV),[24–26] polymer blends (PLA-PCL),[27] or polymer–ceramic composites[28–30] are used in the scaffold fabrication for bone tissue engineering applications. PHBV which is an aliphatic polyester produced by microorganisms is a widely used co-polymer in tissue engineering applications due to its nontoxic, biocompatible, biodegradable, and good spinnability into a nanofibrous structure features.[30,31] However, PHBV polymers are hydrophobic, and their abiotic hydrolysis is relatively slow.[32] Therefore, PHBV can be used in combination with other polymers such as PLLA, gelatin, collagen, chitosan, and silk to enhance degradability,[26,30] hydrophilicity, and biocompatibility.[26,30,33–36]

In the present study, novel three-dimensional nanofibrous cotton wool-like fish scale/PHBV composite scaffolds were fabricated as a bone-filling material for bone regeneration. Composite scaffolds with interconnected porous structure were produced by the addition of chopped fish scales into suspended wet-electrospun PHBV nanofibers and freeze-drying. Scanning electron microscopy (SEM), Fourier transform infrared spectroscopy (FTIR), X-ray diffraction (XRD), and thermogravimetric and differential thermal (DTA/TGA) analyses were used for the characterization of the structure and morphology of the fish scales and the scaffolds. The biocompatibility of the decellularized fish scales and the scaffolds was evaluated in terms of *in vitro* cell culture tests using MG-63 human osteosarcoma cells by resazurin cell proliferation, alkaline phosphatase (ALP) activity, and lactate dehydrogenase (LDH) assays. The scaffolds were also characterized mechanically, histologically, and immunohistochemically. Besides, Ca–P mineral formation tendency of the scaffolds was evaluated by the biomineralization studies. To the best of our knowledge, this is the first time fish scales were incorporated into the three-dimensional nanofibrous scaffold for bone regeneration. Even though fish scales are biodegradable waste materials, structural and compositional similarity to bone ECM are very valuable for bone regeneration. Besides, they are rigid materials that can enhance the mechanical properties of the nanofibrous scaffolds. As a result, the usage of a fish scale in the production of a cost-effective scaffold with a high-added value would be a promising approach for bone regeneration.

Materials and methods

Materials

PHBV (PHV content 3 wt%, $M_n = 80$ kDa) was purchased from Helian Polymers. Benzyl triethylammonium chloride (BTEAC) and chloroform were obtained from Sigma-Aldrich. *Sparus aurata* fishes were obtained from a commercial dealer in Izmir. Tris hydrochloride (Tris–HCl), ethylenediaminetetraacetic acid (EDTA), and sodium dodecyl sulfate (SDS) were used for the decellularization of fish scales and supplied from Applichem. Materials used for cell culture studies are as follows: MG-63 osteosarcoma human cells (ATCC-CRL 1427 Lot number: 57840088, Manassas, VA, USA), MEM-Eagle (MEM; Biological Industries), fetal calf serum (FCS) and L-glutamine (Sigma-Aldrich), Pen-Strep-Ampho (Biological Industries), resazurin assay (Cell signaling, 11884), ALP kit (Enzyline PAL Optimise; Biomerieux, France), and LDH kit (Cytotoxicity detection kit-Roche). Alexa Fluor® 488 (Thermo Fisher Scientific, Molecular Probes) and DAPI (4′, 6-diamidino-2-phenylindole) (Cell Signaling Technology) were used for fluorescence staining. Materials used for histological studies are as follows: hematoxylin (Surgipath, cat.no. 01562E, UK), eosin (Surgipath, cat.no. 01602E, UK), Masson Trichrome staining kit (2049 GBL, Istanbul, Turkey), Alizarin red (Millipore, Billerica, Massachusetts, USA), type I collagen antibody (Bioss bs0578-R), type II collagen antibody (Abcam Collagen II, ab34712), Ultra V Block solution (TA-125-UB, Invitrogen, Fremont, CA), anti-mouse biotin–streptavidin hydrogen peroxide secondary antibodies (Invitrogen-Plus Broad Spectrum 85–9043), 3,3′-diaminobenzidine (DAB) chromogen (Roche, Germany), and Dakopen (Dako, Denmark).

Decellularization of fish scale

Sparus aurata fresh scales were harvested and subsequently cleaned in distilled water several times. Fish scales were first incubated in 10 mM Tris–HCl buffer and %0.1 EDTA at 4°C for 24 h, and then they were left in 0.1% SDS for three days to remove the cellular components of the fish scales. Finally, the scales were

rinsed with 70% ethanol for sterilization and stored in sterilized phosphate-buffered saline (PBS) at 4°C before further application.

Characterization of the fish scales

The morphology of the fish scales was observed by SEM (JEOL JSM-6060). All the samples were sputter-coated (Quorum Technologies, SC7620) with a thin layer of gold/palladium prior to imaging.

Attenuated total reflectance–FTIR (Perkin Elmer Spectrum BX) was used to determine the chemical structures of the fish scales in the wavenumber range of 4000–550 cm^{-1} with the resolution of 4 cm^{-1} and 25 scans/sample.

Crystallinity behavior of the fish scales was determined by Rigaku D/Max. 2200/RC Model XRD with Cu Kα radiation (1.5406 Å) using a 0.05° step size and a 2-s dwell time.

Biocompatibility of the decellularized fish scales

MG-63 osteosarcoma human cells were cultured in MEM that was supplemented with 10% FCS, L-glutamine, and Pen-Strep-Ampho at 37°C in a humidified 5% CO_2 atmosphere. The medium was changed three times weekly. After 89–90% confluence was reached, the cells were trypsinized with trypsin/EDTA buffer.

The cells were seeded on each sterilized (with 70% ethanol) fish scale (size: $3.5 \times 3 \times 1$ mm (L × W × H); $n = 6$) at a density of 1×10^6 cells/ml. After cell attachment, the culture medium was added, and the cells on the scales were cultured for up to 12 days. The same amount of cells was seeded on tissue culture plastic used as a negative control.

Cytotoxicity assay. LDH activity was used as an indicator of cell membrane integrity. Cytotoxicity resulting from residual chemical compounds or processing methods was assessed using a kit commercially available by a spectrophotometer (BioTek, Instruments Winooski, VT, USA) at a reference wavelength of 450 nm. Nine replicates were used per sample.

Proliferation assay. The cell proliferation on fish scales was determined by resazurin assay for measuring cellular metabolic activity quantitatively. Initially, the medium was removed, and resazurin solution (phenol red-free medium and medium, 9:1) was added. Each cell-seeded scale was incubated for 4 h in standard culture conditions. After incubation, the fluorescent metabolite of resazurin was measured by using a fluorometer (Ex = 530–570 nm, Em = 590–620 nm).

ALP activity assay. ALP activity, which is an early marker for the osteoblastic phenotype, was assessed by a commercially available kit on 3, 7, 11, and 15 days. The osteogenic medium (1 µl/ml L-ascorbic acid and 10 µl/ml β-glycerophosphate in complete medium) was used during the cell culture period. ALP activity was quantified by spectrophotometer (BioTek, Instruments Winooski, VT, USA) according to the kit instruction at a wavelength of 405 nm in the third minute.

Cell nuclei and cytoskeleton staining. Nuclei and cytoskeleton stainings were applied after 12 days of culture period. For fixation of each sample, 500 µl 4% paraformaldehyde was added for 30 min. After washing with PBS, they were permeabilized with 0.1% Triton X-100. Samples were incubated with DAPI and Alexa Fluor® 488 at room temperature to visualize the nuclei and the cytoskeleton, respectively. The stained cytoskeleton and nuclei of cells were observed under a fluorescence microscope (ZEISS–OBSERVER Z1).

Preparation of fish scale/PHBV composite scaffolds

PHBV nanofibers were fabricated by wet-electrospinning technique. Initially, PHBV solution was prepared by dissolving PHBV (3% (w/v)) including an organosoluble salt BTEAC (0.2% (w/v)) in chloroform at 50°C for 2 h. PHBV solution was wet-electrospun into a coagulation bath filled with ethanol–water mixture (9:1 v:v) by using a syringe pump (NE-1000, New ERA Pump System, Inc., USA) and high voltage supply (Gamma High Voltage ES30). As a coagulation bath, glass container with a diameter of 25 cm was used, and Cu plate was replaced underneath to maintain the electric field. Electrospinning parameters were as follows: 22-gauge stainless steel needle, 10 cm working distance, 2.0 ml/h flow rate, and 20 kV voltage. The process was continued for 15 min, and the collected wet-electrospun nanofibers were washed thoroughly in distilled water.

Fish scales were first fragmented by a laboratory mixer, and then, in a 24 well-plate, 0.02 g of chopped fish scales was mixed with the suspended wet-electrospun PHBV nanofibers by stirring. In order to obtain porous three-dimensional composite scaffolds, the suspension was subjected to freeze-drying (FreeZone Freeze Dry Systems) at –78°C for 24 h.

Characterization of fish scale/PHBV scaffolds

The morphology of the 3D nanofibrous scaffolds was observed by SEM. The average diameter of the fibers was estimated from the SEM micrographs via Image J program. For each sample, the fiber diameter was measured at 25 different points.

The percent porosities of the scaffolds were measured by mercury porosimetry (Quantachrome Corporation, Poremaster 60). The scaffolds were placed in a penetrometer and pressure was increased to 50 psi, and then the pressure was decreased back to atmospheric pressure.

The chemical structures of the scaffolds were analyzed by ATR–FTIR in the wavenumber range of 4000–550 cm^{-1} with the resolution of 4 cm^{-1} and 25 scans/sample.

Thermal analyses of the scaffolds were performed using a DTA/TGA (Shimadzu DTG-60H). Samples were scanned from 25 to 700°C under a nitrogen atmosphere with a heating rate of 10°C/min. Melting (T_m) and decomposition temperatures (T_d) of the scaffolds were estimated.

Mechanical properties of the scaffolds (diameter, 1.5 cm; height, 1 cm) were determined by compression test (TA XT Plus Texture Analyzer with a 5 kg load cell). The samples were compressed at a constant deformation rate of 1 mm/s up to a strain of 80%. Compressive modules of the scaffolds were determined by slope fitting the initial linear region of stress–strain curves. All the experiments were performed at room temperature. The resulting data were reported as the average of six samples.

Biomineralization studies

Biomineralization studies were carried out for the observation of Ca–P mineral formation tendency on the scaffolds. All the scaffolds were placed in falcon conical tubes containing 20 ml simulated body fluid containing ion concentrations nearly equal to human blood plasma (SBF, pH 7.4) which was prepared according to Kokubo and Takadama,[37] and they were incubated in a water bath at 37°C for four weeks. SBF solutions were changed every 48 h. After biomineralization, the scaffolds were washed three times with deionized water to remove residual salts and dried at room temperature in a desiccator. DTA/TGA was used to analyze the thermal properties of the mineralized scaffolds as well as dispersion and presence of Ca–P minerals on the scaffold surface were investigated by SEM–EDX.

In vitro studies of fish scale/PHBV scaffolds

MG-63 human osteosarcoma cells were cultured with MEM which contained 10% FCS, L-glutamine, and Pen-Strep-Ampho at 37°C in a humidified 5% CO_2 atmosphere. The culture medium was changed twice a week during the cultivation. When the cells became confluent, they were trypsinized and seeded (2×10^6 cells/μl) on the scaffolds (size: $1 \times 1.5 \times 1$ cm ($L \times W \times H$); $n = 6$). MG-63 cells were used for the control group. MG-63 cells were evaluated by LDH, resazurin cell proliferation, and ALP activity assays on days 3, 7, 11, and 15. Additionally, attachment of the cells on the scaffolds was observed by SEM and fluorescence microscopy as mentioned above.

Histologic analysis

Histologic staining was performed to demonstrate cellularity and ECM deposition including hematoxylin and eosin (H&E, for general morphology), masson trichrome (for collagen organization), and immunohistochemistry (for type I and II collagens).

The samples were fixed in 10% formalin solution for 48 h and then embedded in paraffin blocks. Following the routine light microscopic tissue tracking process, 5-μm thick cross-sections were prepared, and the sections were mounted on the glass slides, rehydrated, and stained by either H&E or Masson's trichrome dyes.

Immunohistochemical stainings were performed by type I collagen and type II collagen antibodies. The scaffold cross-sections were first deparaffinized and then rehydrated in decreasing alcohol series. Their surroundings were limited with dakopen without damaging the tissue. About 3% hydrogen peroxide was applied for 10 min to the tissue which was kept waiting in trypsin at 37°C for 15 min in order to inhibit the endogenous peroxidase. Type I collagen primary antibody was applied without washing to the cross-sections, which were washed with PBS, after incubation with blocking solution at room temperature for 30 min and kept waiting at 4°C overnight. After that, the cross-sections were first incubated with a biotinylated secondary antibody and then with avidin–biotin complex (streptavidin) for 30 min each. DAB was used in order to make the reaction visible. Ground staining was made with Mayer's hematoxylin, and after the process of dehydration and making pellucid, they were closed with Entellan.

Statistical analysis

The experimental data are presented as the mean ± standard deviation. In biocompatibility analyses, the differences between groups were analyzed using a two-way analysis of variance (ANOVA) with Tukey's multiple comparison tests. Mechanical test data were carried out using One-way ANOVA with Tukey's multiple comparison tests. All p-values less than 0.05 were considered to be significant.

Results and discussion

Characterization of the fish scales

SEM images of the untreated, decellularized and chopped decellularized fish scales are illustrated in Figure 1. SEM images presented microchannel like

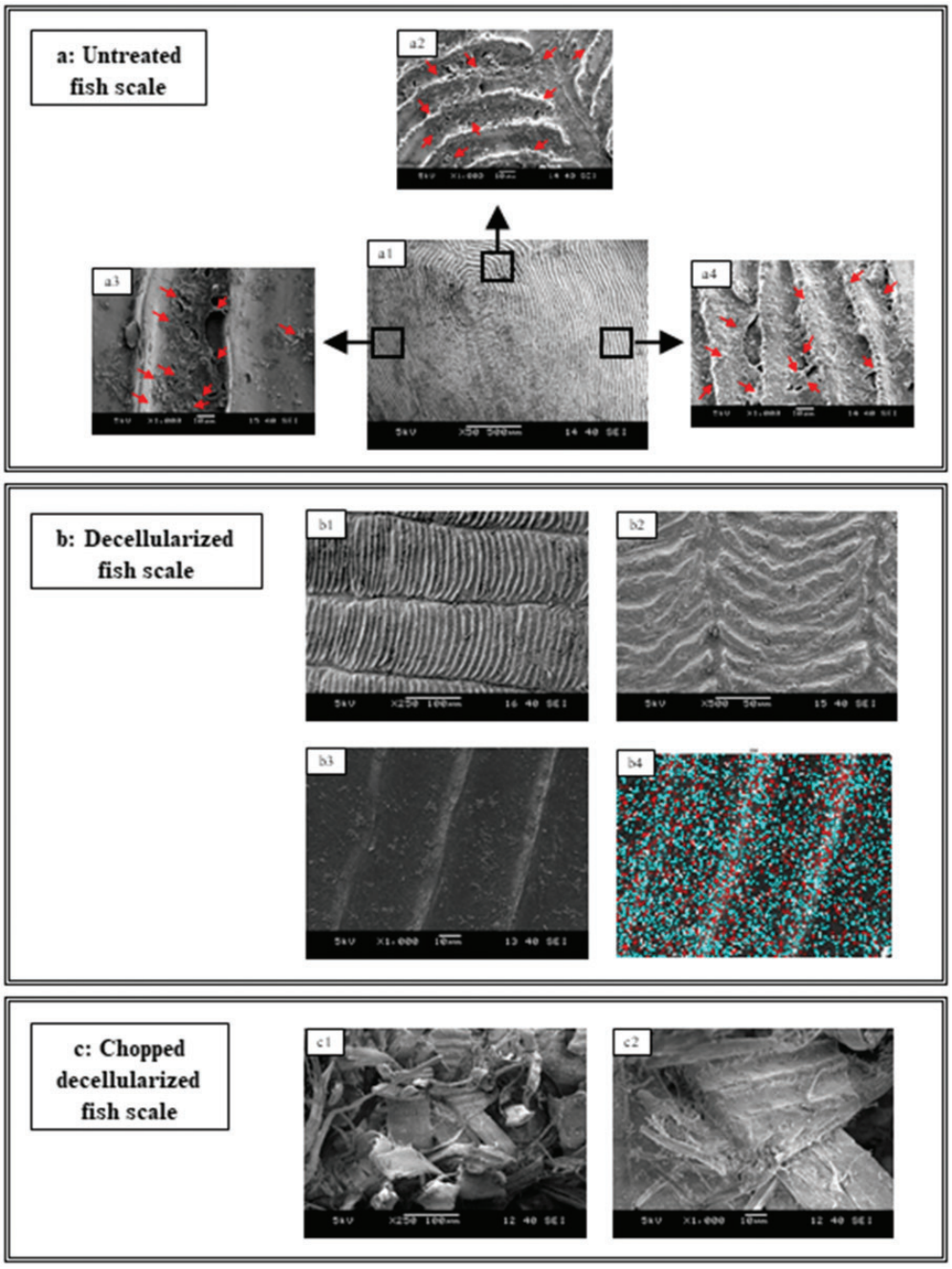

Figure 1. (a) SEM images of the untreated fish scale at 50× (a1) and at 1000× magnifications taken from different regions (a2, a3, a4). Red arrows indicate the cells. (b) SEM images of the decellularized fish scale at 250, 500, and 1000× magnifications (b1, b2, b3) and EDX-mapping image (b4) of the fish scale at 1000× magnification (red spots = Ca, cyan spots = P). (c) SEM images of the chopped decellularized fish scale at 250 and 1000× magnifications.

structures of the fish scales. Figure 1(a) shows three different microchannel orientations of an untreated fish scale from different regions. These microchannels consist of apatite particles embedded in collagen fibers.[6] The cells were clearly observed on the surface of the untreated fish scales along the collagen fibers. After the decellularization process, the cells were successfully removed from the fish scales without any deformation of the structure (Figure 1(b1) to (b3)). Mapping image shows the homogenous distribution of the apatite particles within the collagen matrix in the decellularized fish scale (Figure 1(b4)). Figure 1(c) shows the images of the chopped decellularized fish scales where the fibrillary structures of the collagen

layers fragmented into smaller pieces by preserving the main natural architecture.

FTIR analysis was performed to examine the effect of decellularization and chopping processes on the chemical structure of the fish scales. Figure 2(a) shows the ATR–FTIR spectra of the fish scales. Main characteristics bands of collagen appeared at 3288 cm^{-1} (amide A, related to N–H stretching vibration) and 1632 cm^{-1} (amide I, associated with the stretching vibration of the carbonyl group in peptides). Besides, the amide II and amide III bands associated with N–H bending and C–N stretching vibrations were seen at 1541 cm^{-1} and 1238 cm^{-1}, respectively.[38] The peak at around 1015 cm^{-1} was assigned to P–O stretching band and 600 and 570 cm^{-1} bands that of P–O bending modes of the phosphate group of HAp.[39] The peak intensities of the untreated fish scale which was covered by the cellular components were found to be lower than the treated fish scales. On the other hand, the FTIR spectra of the decellularized and chopped fish scales were almost the same, so it can be concluded that decellularization and chopping processes did not affect the chemical structure of the fish scales.

XRD diffraction patterns of the fish scales are given in Figure 2(b). Reflections at $2\theta = 21.8°$ (200), 25.8° (002), 32.1° (112), and 53.1° (004) were due to the HAp structure (JCPDS no: 00–009-0432) and the broad characteristic peak of collagen appeared at $2\theta = 10°–25°$.[10,40]

In vitro biocompatibility studies of the fish scales

MG-63 cells cultured on the decellularized fish scales were evaluated by cell proliferation assay, ALP activity, and cytotoxicity assay at 4, 7, 10, and 12 days of culture as shown in Figure 3.

The viability of the MG-63 cells on the fish scales was evaluated by resazurin assay (Figure 3(a)). Resazurin reagent is reduced to highly fluorescent resazurin by dehydrogenase enzymes in metabolically active cells. This conversion only occurs in viable cells, and thus, the amount of resazurin produced is proportional to the number of viable cells on the fish scales. As shown in the cell viability results, it was seen that cells proliferated increasingly on the decellularized fish scale, and the increment in the cell viability was statistically significant from days 4 to 12. There was also a statistically significant difference between the decellularized fish scale and the control group at each incubation time. In accordance with the literature results, it can be concluded that fish scales promoted cell attachment and proliferation due to its natural composition and three-dimensional microchannel structure.[7,41,42]

ALP activity was measured in order to evaluate the bone forming ability of the osteoblast cells grown on the fish scales. ALP is an important biochemical factor which used as an early marker of osteoblast phenotype, associated with the synthesis and deposition of type I collagen and non-collagenous bone matrix proteins.[43–45] Similar to the cell viability results, the ALP activity of the MG-63 cells on the decellularized fish scale was increased compared to that of control group during the culture period. ALP activity was significantly higher on the decellularized fish scales after 12 days of culture compared with the other days (Figure 3(b)).

Cytotoxicity of the fish scales decreased gradually during the culture period, and significant differences were observed between days 4 and 10, 4 and 12 as well as days 7 and 12 (Figure 3(c)). It was observed

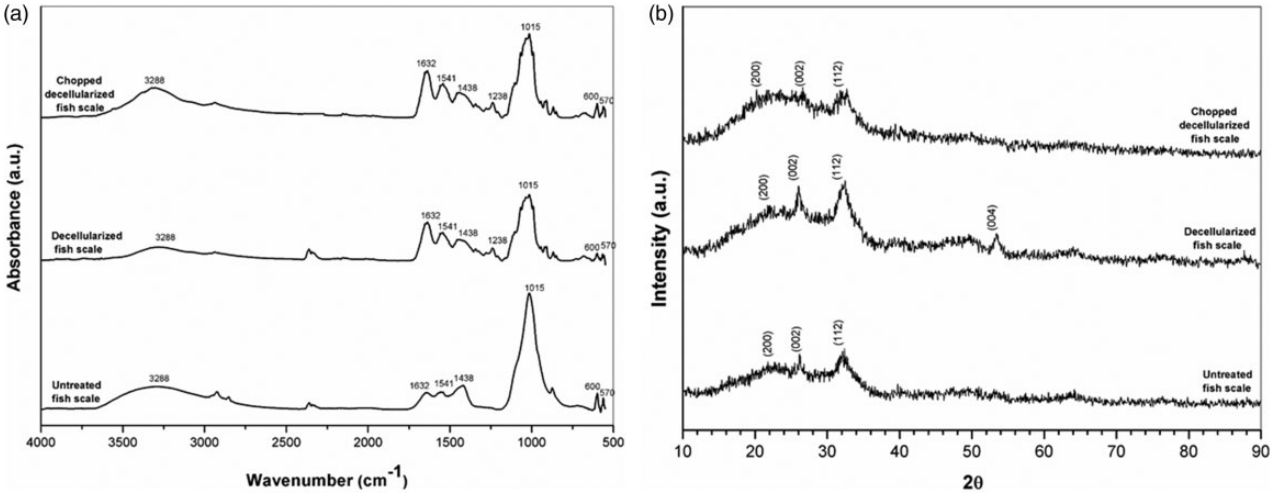

Figure 2. (a) ATR–FTIR spectra and (b) XRD patterns of the untreated, decellularized, and chopped decellularized fish scales.

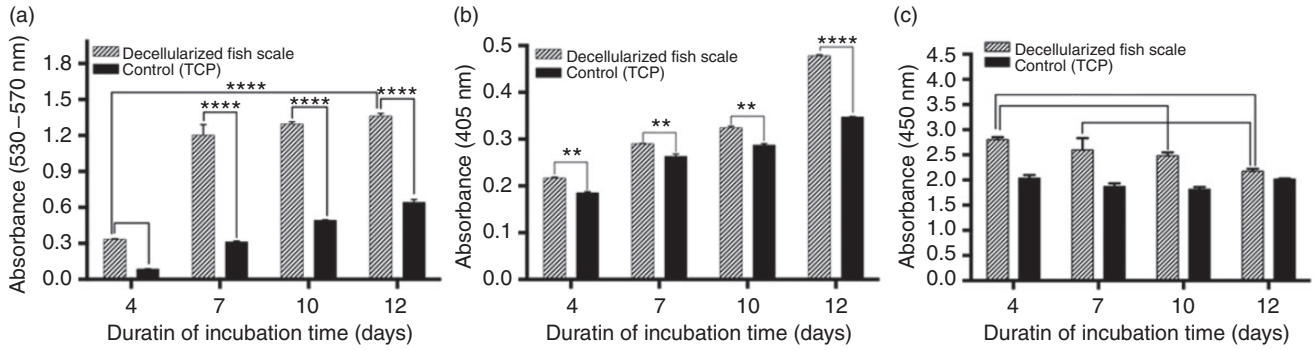

Figure 3. *In vitro* biocompatibility of the decellularized fish scales: (a) proliferation, (b) ALP activity, and (c) cytotoxicity of MG-63 cells on fish scales during 12 days of cell culture (**$p < 0.0086$, ****$p < 0.0001$).

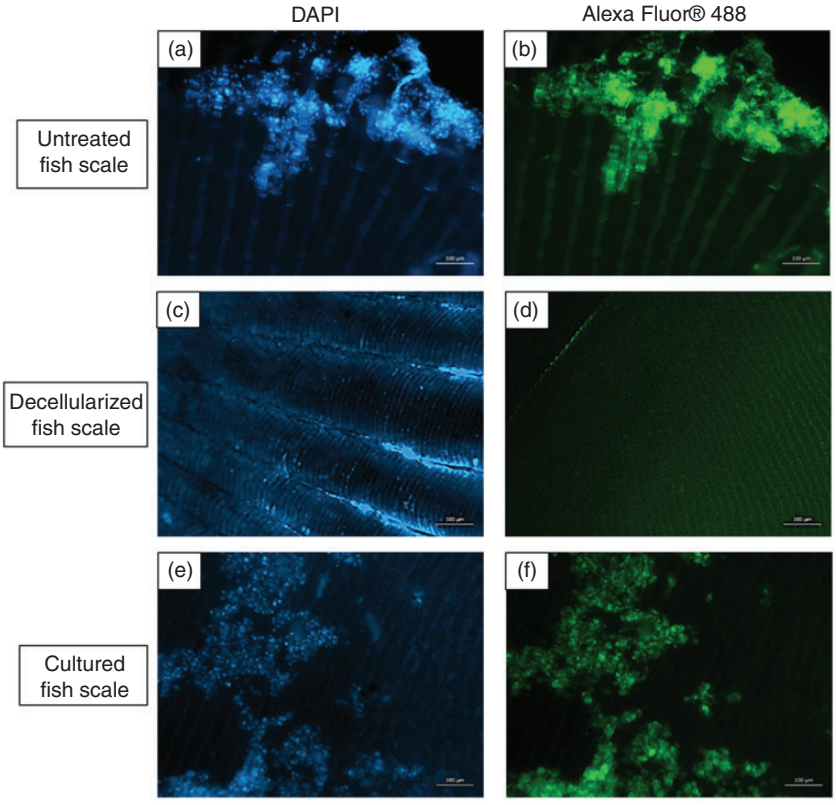

Figure 4. Fluorescence images of untreated, decellularized, and cultured fish scales after 12 days of cell culture. Blue fluorescence reflects staining with DAPI (a, c, and e) and green fluorescence reflects staining with Alexa Fluor® 488 (b, d, and f).

that LDH released from the cells were significantly higher than the control group ($p < 0.001$). The higher LDH level in the early days of the culture is acceptable due to an interaction between the cells and the fish scales on the direct cell culture.

According to our *in vitro* biocompatibility results, despite higher levels of LDH release from the cells during the early culture days in fish scales, gradually increased cell proliferation, and ALP activities showed that fish scales are favorable materials for bone regeneration.

Cell nuclei and cytoskeleton staining

Nuclei and actin filament staining results by DAPI and Alexa Fluor® 488 of the fish scales are shown in Figure 4. Fluorescence images of the fish scales revealed cell nuclei with blue fluorescence and actin filament with green fluorescence. Figure 4(a) and (b) shows the distribution of the cells on the microchannel structure of the untreated fish scale. On the other hand, after the decellularization process, no cells were seen on the decellularized fish scales, as expected (Figure 4(c)

and (d)). The image of the cultured fish scale (Figure 4 (e) and (f)) showed that round-shaped MG-63 cells attached and formed clusters on the fish scale surface after 12 days of culture. Fluorescence staining results indicated that the decellularization process was successfully achieved as parallel to SEM results and decellularized fish scale can provide a suitable environment for cell attachment and spreading due to its natural components and microchannel structure.[18]

Characterization of the fish scale/PHBV scaffolds

The photos of the PHBV and fish scale/PHBV composite scaffolds with a cotton-wool like structure are shown in Figure 5(a) and (d), respectively. It is clearly seen from the cross-section of the composite scaffold that fish scales were successfully embedded within the structure (Figure 5(d)).

SEM images of PHBV (Figure 5(b) and (c)) and fish scale/PHBV composite scaffolds (Figure 5(e) and (f)) showed bead-free three-dimensional nanofibrous morphology. The composite scaffold had chopped decellularized fish scales that were trapped within the nanofibers (Figure 5(e) and (f)). The average fiber diameters of the scaffolds are given in Table 1, and they were between 480–625 nm. The porosity values obtained from the mercury porosimeter were 84.5 and 81.9% for PHBV and composite scaffolds, respectively.

Compressive mechanical properties of the scaffolds were determined by compressive test. Compressive modules of the scaffolds were calculated from the initial linear part of the stress-strain curves. Fish scale/PHBV scaffold is an example of a large-particle reinforced composite in which rigid fish scales increased the compressive modulus of the PHBV scaffold about 2.5-fold (Figure 6(a)). Sultana also showed the improvement of the mechanical properties of PHBV scaffold with the incorporation of HAp particles.[46]

ATR–FTIR spectra of the chopped decellularized fish scale, PHBV, and fish scale/PHBV composite scaffolds are seen in Figure 6(b). C=O stretching vibration of PHBV appeared at 1721 cm^{-1} and C–O stretching bands were at 1278 and 1055 cm^{-1}. C–H stretching band was at around 2978 cm^{-1} besides C–H bending vibrations were at 1453 and 1380 cm^{-1}. The characteristic collagen bands of the fish scales which were

Table 1. Average fiber diameters of the scaffolds.

Scaffold	Fiber diameter (nm)
PHBV	552 ± 70
Fish scale/PHBV	560 ± 64

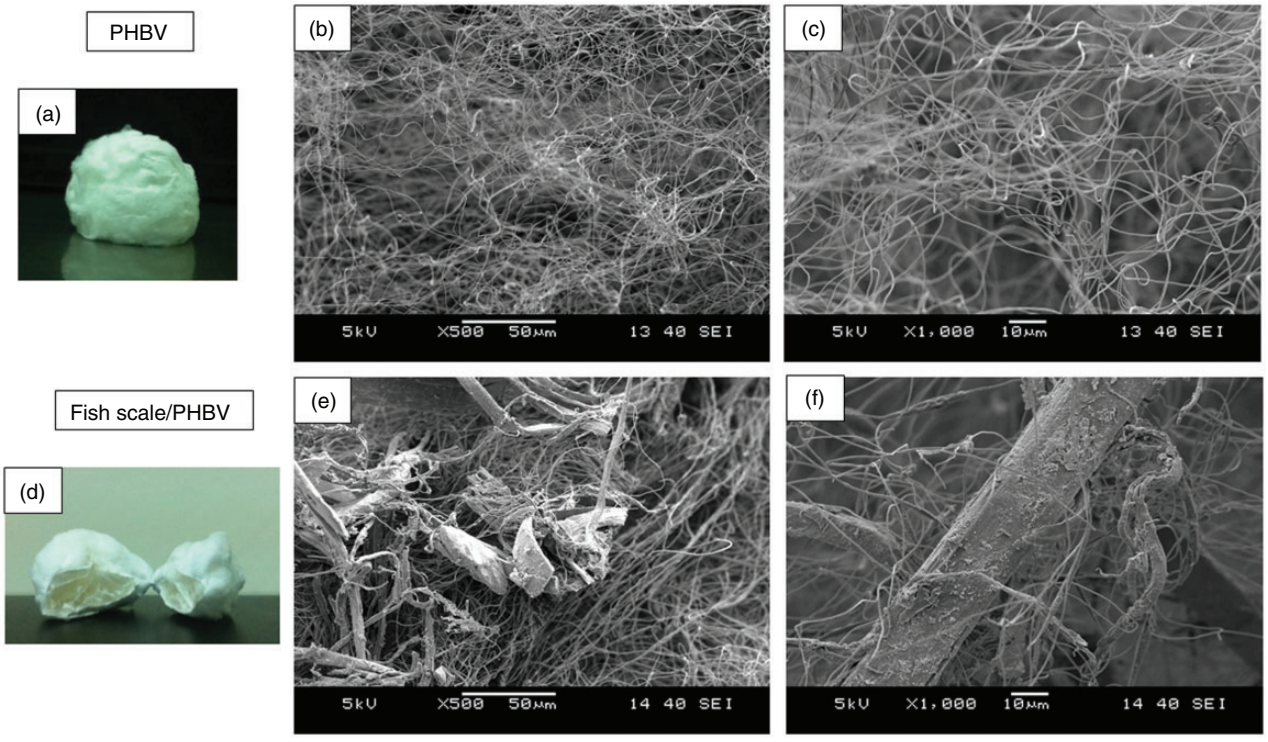

Figure 5. Macroscopic image (a) and SEM images of the PHBV scaffold (b and c); macroscopic cross-section image (d) and SEM images of fish scale/PHBV composite scaffold (e and f).

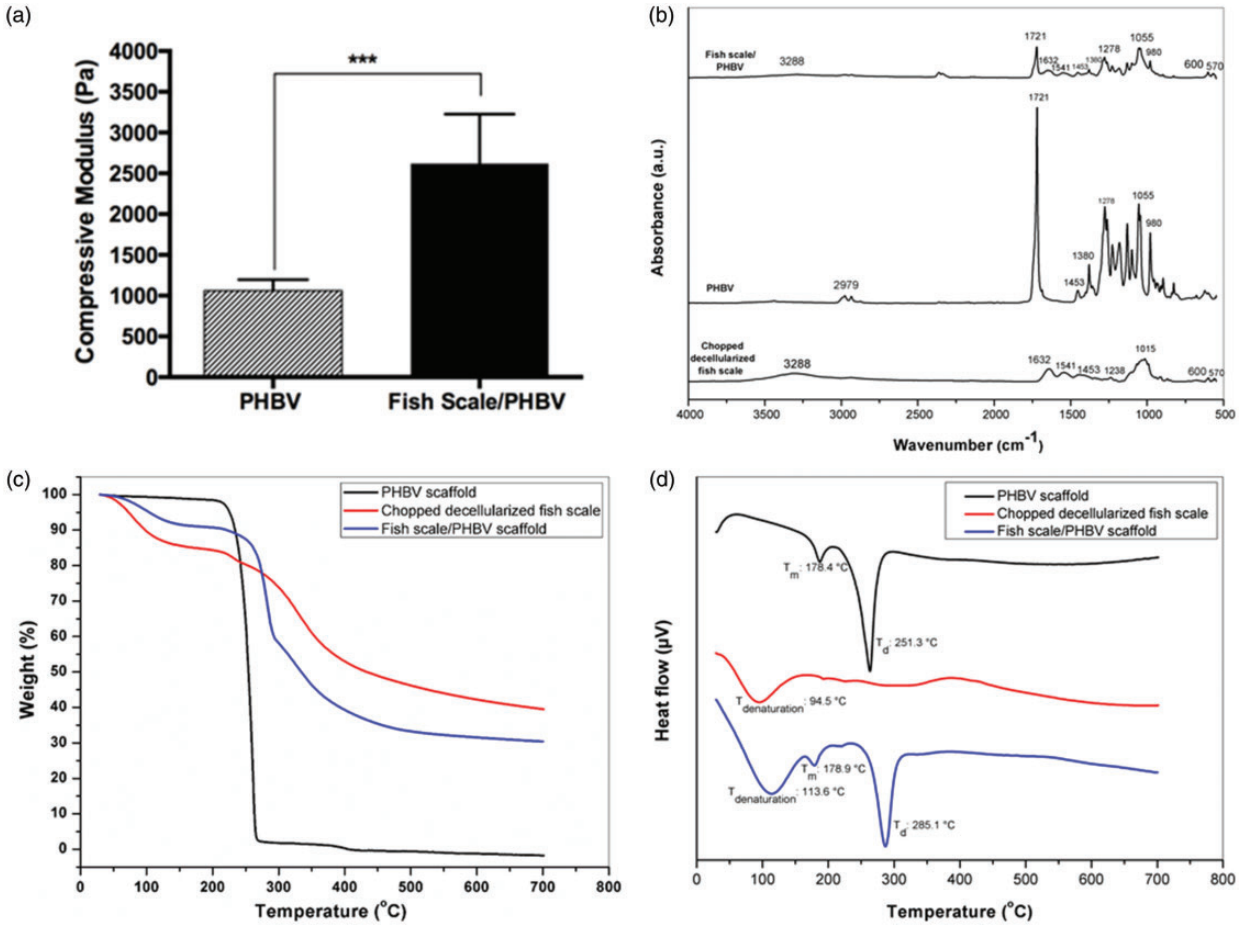

Figure 6. (a) Compressive modulus of the PHBV and fish scale/PHBV composite scaffolds (***$p < 0.001$); (b) ATR–FTIR spectra, (c) TGA, and (d) DTA curves of the chopped decellularized fish scale, PHBV, and fish scale/PHBV composite scaffolds.

assigned to amide A, amide I, amide II, and amide III appeared at around 3288, 1632, 1541, and 1238 cm^{-1}, respectively. Besides, P–O stretching band at around 1015 cm^{-1} and P–O bending bands at 600 and 570 cm^{-1} due to HAp were also present. In the spectra of fish scale/PHBV scaffold, both characteristic peaks of PHBV and fish scale are seen which proved that the fish scales were successfully incorporated into the PHBV nanofibers.

Thermal characterization of the chopped decellularized fish scale, PHBV, and fish scale/PHBV composite scaffolds was performed by DTA/TGA. In Figure 6(c), TGA curve of the PHBV scaffold showed a single-stage decomposition between 210 and 270°C due to scission of the polymer chains, whereas fish scale and fish scale/PHBV scaffold showed two-stage decomposition assigned to loss of adsorbed water followed by thermal decomposition of the polymer matrix. From the TGA curve of the chopped decellularized fish scale, HAp content was found as 40 wt%. The actual weight percentage of HAp in the composite scaffold was determined as 30 wt% which is close to the theoretical composition of HAp (27 wt%) meaning that fish scales were distributed well within the scaffolds. As shown in the DTA curves (Figure 6(d)), the denaturation temperature of collagen and the T_m value of PHBV was found as 95 and 178.4°C, respectively. T_d value of PHBV scaffold was at around 251.3°C; however, fish scale/PHBV scaffold displayed improved thermal stability with a higher T_d value of 280.4°C.

Biomineralization studies

Biomineralization studies in SBF have been regarded as an evidence for the *in vitro* bioactivity of materials.[47] Therefore, the biomineralization ability of the scaffolds was investigated by incubating the scaffolds in SBF solution at 37°C for four weeks.

The morphological analysis of the mineralized scaffolds was performed with SEM, and dispersion and the presence of Ca-P minerals were analyzed with EDX mapping. Figure 7(a) to (d) shows the SEM images

of the PHBV and fish scale/PHBV composite scaffolds after two and four weeks of incubation in SBF. On PHBV scaffolds, no Ca–P mineral formation was observed within the incubation time (Figure 7(a) and (b)). Only, the average fiber diameters of the scaffolds increased slightly from 552 ± 70 nm to 555 ± 83 nm and 600 ± 71 nm at the end of two and four weeks of biomineralization, respectively. On the other hand, after two weeks in SBF, Ca–P mineral clusters appeared especially on the fish scales of the composite scaffold (Figure 7(c)). Furthermore, an increased amount of Ca–P minerals was observed throughout fish scale/PHBV scaffolds after four weeks of incubation (Figure 7(d)). EDX-mapping results revealed the uniform distribution of Ca and P minerals for the fish scale/PHBV scaffold after two (Figure 7(e)) and four (Figure 7(f)) weeks of incubation. Consequently, SEM and EDX-mapping results confirmed that PHBV alone have no ability to induce bone-like mineral growth due to its hydrophobic nature and lack of sufficient functional groups, while fish scale incorporation promoted the nucleation and adhesion of Ca–P minerals.

Thermal properties of the mineralized scaffolds were investigated using DTA/TGA. TGA curves are shown in Figure 8(a). PHBV scaffolds showed similar trends before and after biomineralization with no distinct inorganic content change. However, the inorganic content of the fish scale/PHBV composite scaffolds increased from 30 to 46 and 56 wt% after two and four weeks of incubation in SBF, respectively. These results suggested that the fish scale played an important role in the nucleation and growth of mineral phase and clearly enhanced the quantity of the deposited minerals on the scaffold surfaces.

The DTA curves of the scaffolds before and after biomineralization are given in Figure 8(b). After incubation in SBF, only the intensity of the peaks of the composite scaffolds assigned to denaturation of collagen and loss of adsorbed water (~100°C), melting of PHBV (~178°C), and the decomposition of the polymer matrix (~280°C) reduced due to deposition of Ca–P minerals.

In vitro studies of the fish scale/PHBV scaffolds

The morphology of the scaffolds is important for cell proliferation. Three-dimensional fibrous and porous

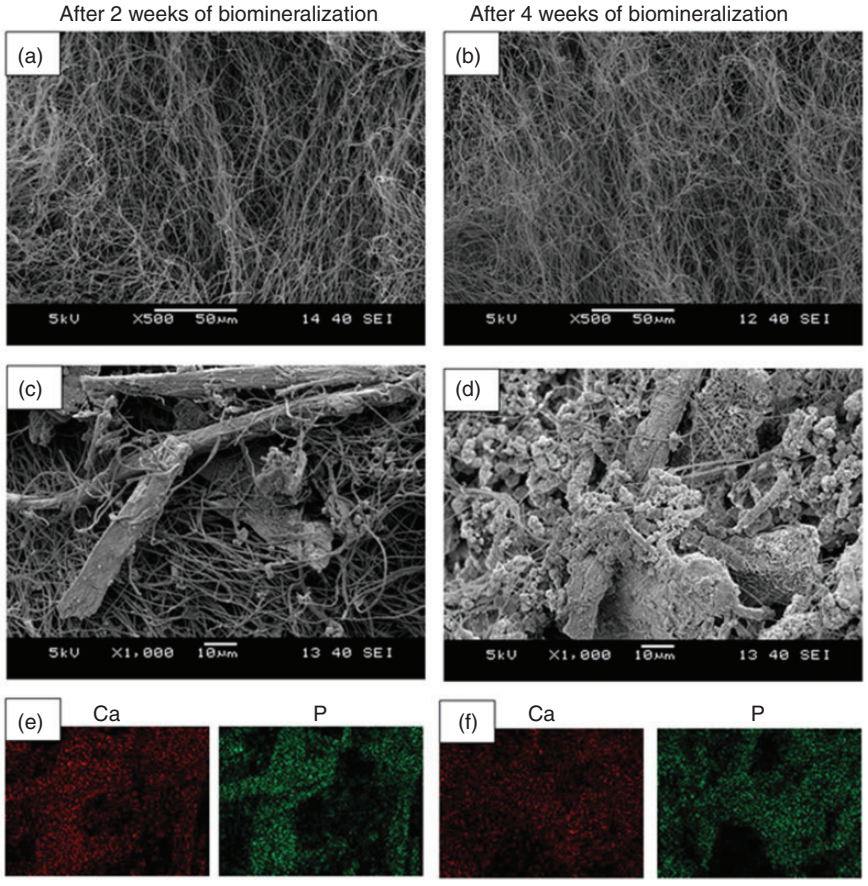

Figure 7. SEM images of the PHBV and fish scale/PHBV composite scaffolds after two weeks (a and c) and four weeks of biomineralization (b and d), and EDX-mapping spectra of fish scale/PHBV composite scaffold after two (e) and four (f) weeks of biomineralization (red spots = Ca, green spots = P; magnification = 1000×).

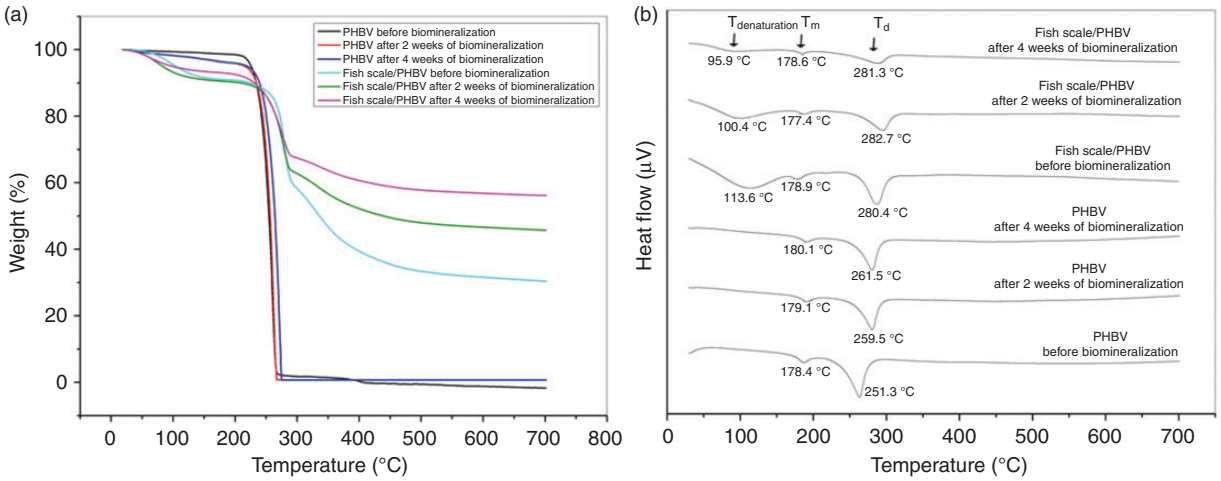

Figure 8. (a) TGA and (b) DTA curves of the PHBV and fish scale/PHBV composite scaffolds before and after two and four weeks of biomineralization.

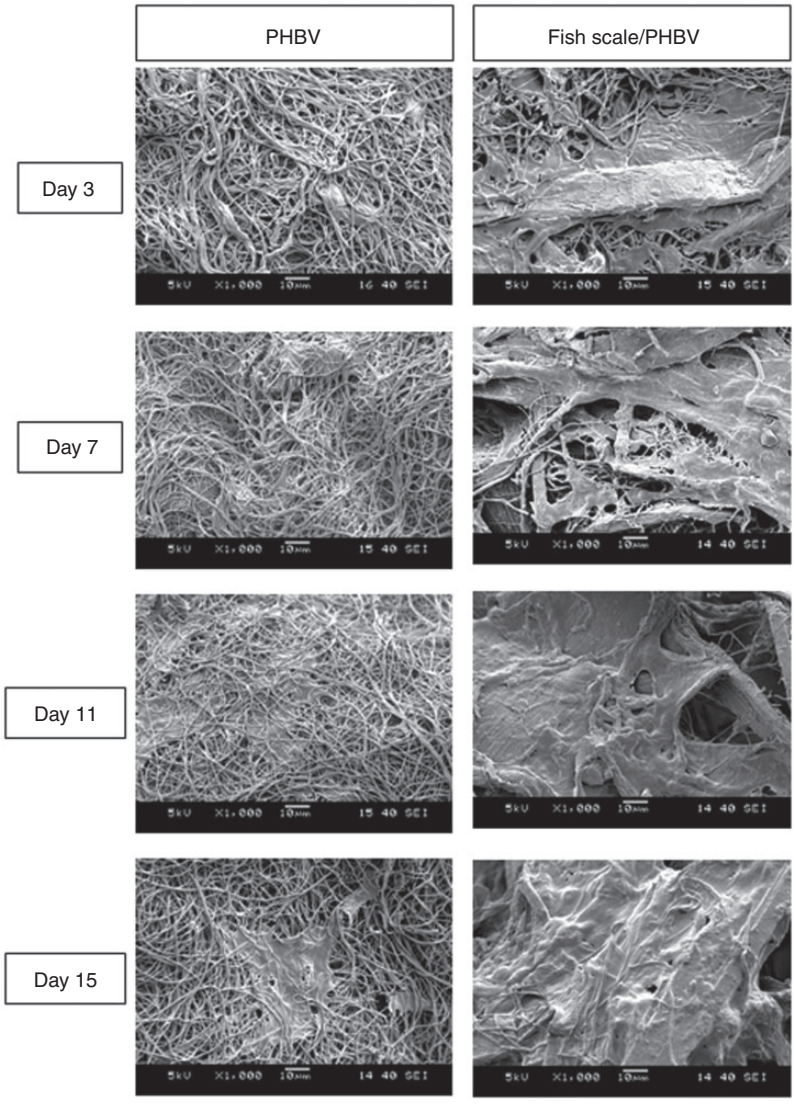

Figure 9. SEM images of the MG-63 cells on the PHBV and fish scale/PHBV composite scaffolds after 3, 7, 10, and 15 days of culture (magnification = 1000×).

morphology of the scaffolds support cell attachment and spreading.[22] The morphologies of the PHBV and fish scale/PHBV composite scaffolds after cell culture were observed with SEM and depicted in Figure 9. MG-63 cells attached and spread on both of the scaffolds during the culture period due to their fibrous and porous morphologies. It can be easily seen that osteoblast cells exhibited a flattened morphology extended in all directions on the scaffolds. However, MG-63 cells were well attached and spread on the fish scale/PHBV composite scaffold compared to the PHBV scaffold especially on day 15 due to the presence of collagen and HAp in the fish scales.

The viability of MG-63 cells on the scaffolds was evaluated by resazurin assay. Figure 10(a) shows cell viabilities at 3, 7, 11, and 15 days of cultivation. The cells proliferated gradually on all the scaffolds during the culture period. Significant differences in absorbance values for each of the scaffolds were detected between days 3 and 15. Besides, the cell viability results of fish scale/PHBV composite scaffolds were found to be statistically significant on days 11 and 15 when compared to PHBV scaffolds.

Figure 10(b) shows the ALP activity of MG-63 cells cultured on the scaffolds for 3, 7, 11, and 15 days. The ALP values of the scaffolds measured on culture days 3 and 7 were not statistically significant. However, ALP activity increased in all groups on day 15 compared to day 3. The cells on the fish scale/PHBV composite scaffolds showed statistically the highest ALP activity after 11 and 15 days of incubation. Similar to our results, it was stated in the literature that osteoblasts cultured on scaffolds had enhanced ALP activity with the incorporation of HAp, and this enhancement was more pronounced at prolonged cell culture times.[48]

For evaluation of scaffolds' cytotoxicity, LDH assay was performed at 3, 7, 11, and 15 days after cell culture (Figure 10(c)). LDH levels released from the cells on day 3 were higher in both of the scaffolds similar to the cytotoxicity results of the fish scales (Figure 3(c)). However, on day 11, none of the scaffolds showed a statistically significant difference in terms of LDH release from MG-63 cells. There was also no significant difference between the fish scale/PHBV composite scaffold and control group on day 15.

MG-63 cells cultured on PHBV and fish scale/PHBV composite scaffolds for 15 days were stained with DAPI and Alexa Fluor® 488 and visualized by fluorescence microscopy (Figure 11). Fluorescence microscopy images showed that MG-63 cells spread more on the fish scale/PHBV composite scaffolds compared to PHBV scaffold.

According to *in vitro* biocompatibility study results of the fish scale/PHBV composite scaffolds, incorporation of fish scale improved the biocompatibility of the scaffolds for bone regeneration.

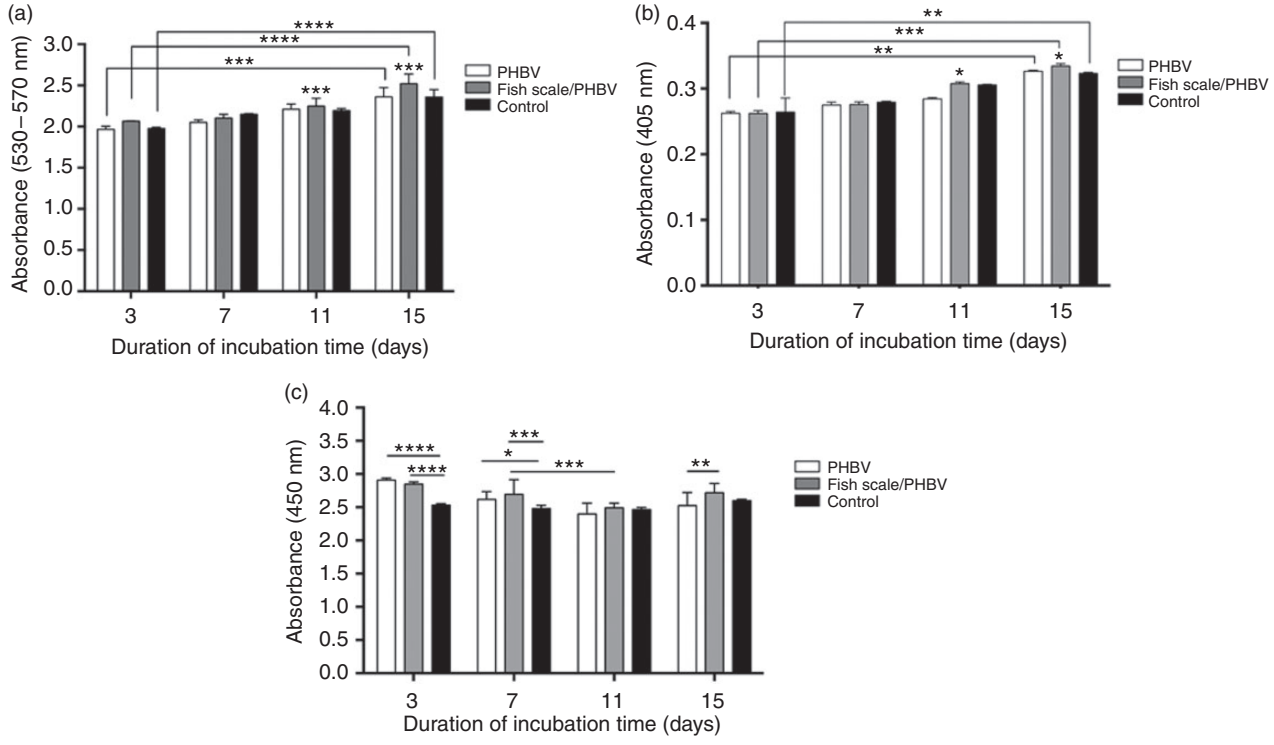

Figure 10. *In vitro* biocompatibility of the PHBV and fish scale/PHBV composite scaffolds: (a) proliferation, (b) ALP activity, and (c) cytotoxicity of MG-63 cells on the scaffolds during 15 days of cell culture (*$p < 0.05$; **$p < 0.01$; ***$p < 0.001$; ****$p < 0.0001$).

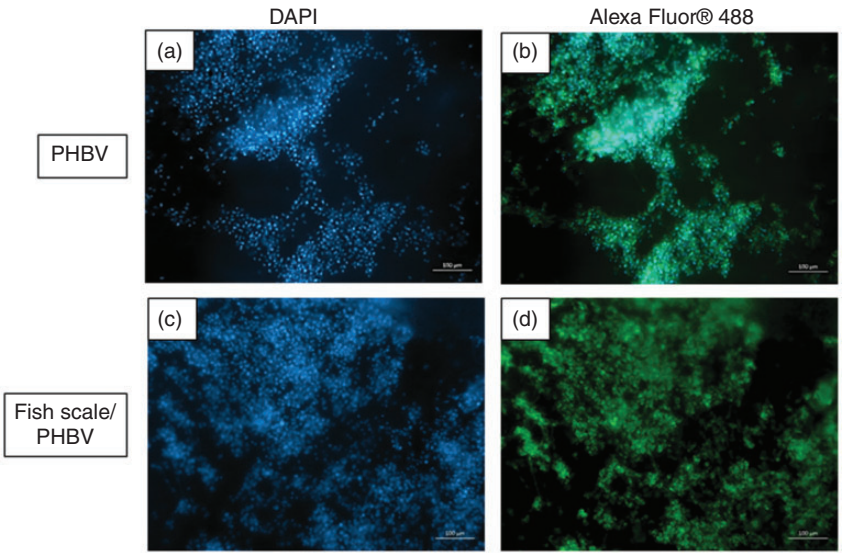

Figure 11. Fluorescence images of the PHBV and fish scale/PHBV composite scaffolds after 15 days of cell culture. Blue fluorescence reflects staining with DAPI (a and c) and green fluorescence reflects staining with Alexa Fluor® 488 (b and d).

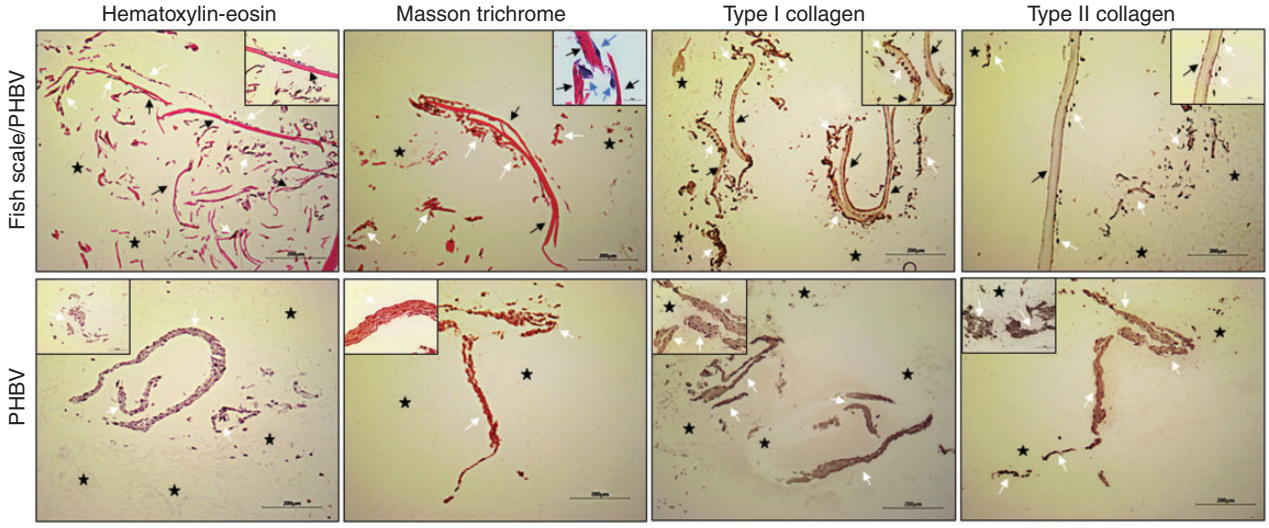

Figure 12. Histological and immunohistochemical stainings of the fish scale/PHBV composite scaffold after 15 days of cell culture (stars: PHBV nanofibers, white arrow: cells, black arrow: fish scale, blue arrow: connective tissue produced by cells).

Histologic analysis

MG-63 cell proliferation and colonization on the PHBV and fish scale/PHBV composite scaffolds were evaluated by histologic analysis (Figure 12). Histomorphological evaluation by H&E and Masson trichrome staining as well as immunohistochemical analysis of type I and II collagen revealed cell adhesion and proliferation on both of the scaffolds after 15 days of culture. Images also proved that cells infiltrated through the internal regions of the scaffolds. Although PHBV nanofibers do not appear clear in the stainings, cell adhesion within the PHBV scaffold was supported by its nanofibrous structure. However, composite scaffold images showed that MG-63 cells preferred to attach and align along the fish scales within the PHBV nanofibers owing to the collagen and HAp content of the fish scales. Masson trichrome staining indicated collagen deposition around osteoblasts and collagen present in the structure of the fish scales. The images also showed that the addition of the fish scales into the PHBV nanofibers enhanced the production of connective tissue (blue arrows) on the composite scaffolds. Immunohistochemical stainings

revealed that MG-63 cells expressed both type I and type II collagen on PHBV scaffolds. However, on the fish scale/PHBV composite, scaffold expression of type I collagen was more pronounced than type II collagen. Based on these results, that composite scaffolds could assist the regeneration of bone defects.

Conclusion

In this study, the usage of decellularized fish scales within the nanofibrous scaffold was evaluated for bone regeneration. For this purpose, three-dimensional porous cotton wool-like fish scale/PHBV composite scaffold was produced by integrating the chopped decellularized fish scales into the suspended wet-electrospun PHBV nanofibers followed by freeze-drying. Incorporation of the fish scales increased the deposition of the Ca–P minerals as well as compressive modulus of the scaffold. Based on the *in vitro* test results, the composite scaffold exhibited improved bioactivity compared to PHBV scaffold. Consequently, fish scale/PHBV scaffold can be evaluated as a candidate filling material for bone regeneration.

Acknowledgements

The authors would like to thank Izmir Institute of Technology Biotechnology and Bioengineering Research and Application Center for the freeze-drying process and fluorescence microscopy analyses and METU Central Laboratory for the porosity measurements.

Declaration of conflicting interests

The author(s) declared no potential conflicts of interest with respect to the research, authorship, and/or publication of this article.

Funding

The author(s) received no financial support for the research, authorship, and/or publication of this article.

ORCID iD

Aylin Z Albayrak https://orcid.org/0000-0003-4137-5696

References

1. Weigel T, Schinkel G and Lendlein A. Design and preparation of polymeric scaffolds for tissue engineering. *Expert Rev Med Devices* 2006; 3: 835–851.
2. Poologasundarampillai G, Wang D, Li S, et al. Cotton-wool-like bioactive glasses for bone regeneration. *Acta Biomater* 2014; 10: 3733–3746.
3. O'brien FJ. Biomaterials and scaffolds for tissue engineering. *Mater Today* 2011; 14: 88–95.
4. Fernandez-Yague MA, Abbah SA, McNamara L, et al. Biomimetic approaches in bone tissue engineering: Integrating biological and physicomechanical strategies. *Adv Drug Deliv Rev* 2015; 84: 1–29.
5. Qiu Z-Y, Cui Y, Tao C-S, et al. Mineralized collagen: rationale, current status, and clinical applications. *Mater (Basel)* 2015; 8: 4733–4750.
6. Ikoma T, Kobayashi H, Tanaka J, et al. Microstructure, mechanical, and biomimetic properties of fish scales from Pagrus major. *J Struct Biol* 2003; 142: 327–333.
7. Metz J, De Vrieze E, Lock EJ, et al. Elasmoid scales of fishes as model in biomedical bone research. *J Appl Ichthyol* 2012; 28: 382–387.
8. Lin CC, Ritch R, Lin SM, et al. A new fish scale-derived scaffold for corneal regeneration. *Eur Cell Mater* 2010; 19: 50–57.
9. Okuda M, Ogawa N, Takeguchi M, et al. Minerals and aligned collagen fibrils in tilapia fish scales: structural analysis using dark-field and energy-filtered transmission electron microscopy and electron tomography. *Microsc Microanal* 2011; 17: 788–798.
10. Jana P, Mitra T, Selvaraj TKR, et al. Preparation of guar gum scaffold film grafted with ethylenediamine and fish scale collagen, cross-linked with ceftazidime for wound healing application. *Carbohydr Polym* 2016; 153: 573–581.
11. Van Essen T, Van Zijl L, Possemiers T, et al. Biocompatibility of a fish scale-derived artificial cornea: cytotoxicity, cellular adhesion and phenotype, and in vivo immunogenicity. *Biomaterials* 2016; 81: 36–45.
12. Kaczmarek B, Sionkowska A and Osyczka AM. Collagen-based scaffolds enriched with glycosaminoglycans isolated from skin of Salmo salar fish. *Polym Test* 2017; 62: 132–136.
13. Turnbull G, Clarke J, Picard F, et al. 3D bioactive composite scaffolds for bone tissue engineering. *Bioact Mater* 2018; 3: 278–314.
14. Mondal B, Mondal S, Mondal A, et al. Fish scale derived hydroxyapatite scaffold for bone tissue engineering. *Mater Character* 2016; 121: 112–124.
15. Mondal S, Pal U and Dey A. Natural origin hydroxyapatite scaffold as potential bone tissue engineering substitute. *Ceram Int* 2016; 42: 18338–18346.
16. Pon-On W, Suntornsaratoon P, Charoenphandhu N, et al. Hydroxyapatite from fish scale for potential use as bone scaffold or regenerative material. *Mater Sci Eng C Mater Biol Appl* 2016; 62: 183–189.
17. Choi SM, Kang HY, Min H-J, et al. Bioactive fish collagen/polycaprolactone composite nanofibrous scaffolds fabricated by electrospinning for 3D cell culture. *J Biotechnol* 2015; 205: 47–58.
18. Fang Z, Wang Y, Feng Q, et al. Hierarchical structure and cytocompatibility of fish scales from Carassius auratus. *Mater Sci Eng C Mater Biol Appl* 2014; 43: 145–152.
19. Yamamoto K, Igawa K, Sugimoto K, et al. Biological safety of fish (tilapia) collagen. *BioMed Res Int*. Epub ahead of print 7 April 2014. DOI: 10.1155/2014/630757.
20. Jang J-H, Castano O and Kim H-W. Electrospun materials as potential platforms for bone tissue engineering. *Adv Drug Deliv Rev* 2009; 61: 1065–1083.
21. Vasita R and Katti DS. Nanofibers and their applications in tissue engineering. *Int J Nanomed* 2006; 1: 15.

22. Sun B, Long Y, Zhang H, et al. Advances in three-dimensional nanofibrous macrostructures via electrospinning. *Prog Polym Sci* 2014; 39: 862–890.
23. Kostakova E, Seps M, Pokorny P, et al. Study of polycaprolactone wet electrospinning process. *Express Polym Lett* 2014; 8: 554–564.
24. Sadeghi A, Nokhasteh S, Molavi A, et al. Surface modification of electrospun PLGA scaffold with collagen for bioengineered skin substitutes. *Mater Sci Eng C Mater Biol Appl* 2016; 66: 130–137.
25. Qutachi O, Vetsch JR, Gill D, et al. Injectable and porous PLGA microspheres that form highly porous scaffolds at body temperature. *Acta Biomater* 2014; 10: 5090–5098.
26. Ferreira B, Zavaglia C and Duek E. Films of poly (L-lactic acid)/poly (hydroxybutyrate-*co*-hydroxyvalerate) blends: in vitro degradation. *Mater Res* 2001; 4: 34–42.
27. Patrício T, Gloria A and Bártolo PJ. PCL and PCL/PLA scaffolds for bone tissue regeneration. *AMR* 2013; 683: 168–171.
28. Banglmaier RF, Sander EA and VandeVord PJ. Induction and quantification of collagen fiber alignment in a three-dimensional hydroxyapatite–collagen composite scaffold. *Acta Biomater* 2015; 17: 26–35.
29. Calabrese G, Giuffrida R, Fabbi C, et al. Collagen-hydroxyapatite scaffolds induce human adipose derived stem cells osteogenic differentiation in vitro. *PLoS One* 2016; 11: e0151181
30. Sultana N and Wang M. PHBV/PLLA-based composite scaffolds containing nano-sized hydroxyapatite particles for bone tissue engineering. *J Exp Nanosci* 2008; 3: 121–132.
31. Ai J, Heidari KS, Ghorbani F, et al. Fabrication of coated-collagen electrospun PHBV nanofiber film by plasma method and its cellular study. *J Nanomater* 2011; Article ID: 123724.
32. Bastioli C. *Handbook of biodegradable polymers*. Akron, OH: Smithers Rapra Publishing, 2005.
33. Kuppan P, Sethuraman S and Krishnan UM. Poly (3-hydroxybutyrate-co-3-hydroxyvalerate)-based nanofibrous scaffolds to support functional esophageal epithelial cells towards engineering the esophagus. *J Biomater Sci Polym Ed* 2014; 25: 574–593.
34. Bakare RA, Bhan C and Raghavan D. Synthesis and characterization of collagen grafted poly (hydroxybutyrate–valerate) (PHBV) scaffold for loading of bovine serum albumin capped silver (Ag/BSA) nanoparticles in the potential use of tissue engineering application. *Biomacromolecules* 2013; 15: 423–435.
35. Biazar E and Keshel SH. Chitosan–cross-linked nanofibrous PHBV nerve guide for rat sciatic nerve regeneration across a defect bridge. *ASAIO J* 2013; 59: 651–659.
36. Unalan I, Colpankan O, Albayrak AZ, et al. Biocompatibility of plasma-treated poly (3-hydroxybutyrate-co-3-hydroxyvalerate) nanofiber mats modified by silk fibroin for bone tissue regeneration. *Mater Sci Eng C Mater Biol Appl* 2016; 68: 842–850.
37. Kokubo T and Takadama H. How useful is SBF in predicting in vivo bone bioactivity? *Biomaterials* 2006; 27: 2907–2915.
38. Kong J and Yu S. Fourier transform infrared spectroscopic analysis of protein secondary structures. *Acta Biochim Biophys Sin (Shanghai)* 2007; 39: 549–559.
39. Liu W, Zhang Y, Li G, et al. Structure and composition of teleost scales from snakehead *Channa argus* (Cantor) (Perciformes: Channidae). *J Fish Biol* 2008; 72: 1055–1067.
40. Ramanathan G, Singaravelu S, Raja M, et al. Extraction and characterization of collagen from the skin of *Arothron stellatus* fish – a novel source of collagen for tissue engineering. *J Biomater Tissue Eng* 2014; 4: 203–209.
41. Sugiura H, Yunoki S, Kondo E, et al. In vivo biological responses and bioresorption of tilapia scale collagen as a potential biomaterial. *J Biomater Sci Polym Ed* 2009; 20: 1353–1368.
42. Nagai N, Nakayama Y, Zhou YM, et al. Development of salmon collagen vascular graft: mechanical and biological properties and preliminary implantation study. *J Biomed Mater Res Part B Appl Biomater* 2008; 87: 432–439.
43. Li Y, Hu W, Han G, et al. Involvement of bone morphogenetic protein–related pathways in the effect of aucubin on the promotion of osteoblast differentiation in MG63 cells. *Chem Biol Interact* 2018; 283: 51–58.
44. Orimo H. The mechanism of mineralization and the role of alkaline phosphatase in health and disease. *J Nippon Med Sch* 2010; 77: 4–12.
45. Marie PJ. Role of N-cadherin in bone formation. *J Cell Physiol* 2002; 190: 297–305.
46. Sultana N and Khan TH. In vitro degradation of PHBV scaffolds and nHA/PHBV composite scaffolds containing hydroxyapatite nanoparticles for bone tissue engineering. *J Nanomater* 2012; Article ID: 190950.
47. Pawelec KM and Kluijtmans SG. Biomineralization of recombinant peptide scaffolds: interplay among chemistry, architecture, and mechanics. *ACS Biomater Sci Eng* 2017; 3: 1100–1108.
48. Gunes OC, Unalan I, Cecen B, et al. Three-dimensional silk impregnated HAp/PHBV nanofibrous scaffolds for bone regeneration. *Int J Polym Mater Polym Biomater* 2019; 68: 214–228.